## Title

Application of Non-Ergodic Site Response for High Velocity Contrast Sites in the San Francisco Bay Area



## Journal

Japanese Geotechnical Society Special Publication, 10(28)

## ISSN

2188-8027

## Authors

Teague, David
Vahdani, Shahriar
Stewart, Jonathan
et al.

## Publication Date

2024

## DOI

10.3208/jgssp.v10.os-17-06

Peer reviewed

# Application of Non-Ergodic Site Response for High Velocity Contrast Sites in the San Francisco Bay Area

David P. Teague [i], Shahriar Vahdani[ii], Jonathan P. Stewart [iii], and Parham Khoshkbari [iv]

i) Associate, ENGEO Incorporated, 2010 Crow Canyon Place, Suite 250, San Ramon, CA, 94583, USA.
ii) President, Applied Geodynamics, Inc., 1205 Contra Costa Drive, El Cerrito, CA, 94530, USA.
iii) Professor, Civil and Environmental Eng., University of California, Los Angeles, 4731K Boelter Hall, Los Angeles, CA, 90095, USA.
iv) Director of Infrastructure, Real Estate Development, Google, Sunnyvale, CA, USA.

## ABSTRACT

Seismic-hazard analysis (SHA) is typically performed using ergodic ground-motion models (GMMs), wherein the site response component is derived from global data and conditioned on the time-averaged shear-wave velocity in the upper 30 meters ($V_{S30}$) and a "basin depth" term (e.g., $Z_{1.0}$ or $Z_{2.5}$). In the ergodic GMMs, for a given $V_{S30}$, there is an implicit shear-wave velocity ($V_S$) profile associated with the site response prediction that has smooth increases of velocity with depth. When a site-specific $V_S$ profile is characterized by abrupt velocity contrasts, for example at the rock-soil interface, the site response is likely to differ significantly from ergodic model predictions. This limitation of the ergodic models can be overcome by incorporating non-ergodic site response in the SHA. This approach involves customizing the site response for site-specific conditions, which has the effect of decreasing overall model uncertainty.

In this paper, we describe results from ergodic SHA and SHA that incorporates non-ergodic site response at two sites in the San Francisco Bay Area. Both sites are characterized by a strong impedance contrast at the top of competent bedrock. Depth to bedrock at these sites varies, ranging from 75 meters to more than 400 meters. At each of the sites, nearby ground-motion records indicate that the ergodic GMMs tend to underestimate spectral accelerations at oscillator periods that are close to the fundamental site period. Conversely, there are typically broad period ranges where the ergodic GMMs overestimate spectral acceleration. Since the non-ergodic site response considers these local ground-motion data, these differences are reflected in the non-ergodic results. The findings from these two sites underscore the importance of estimating the fundamental site period, the limitations of ergodic models at sites with strong impedance contrasts, and the benefits of implementing non-ergodic site response into SHA.

**Keywords:** non-ergodic site response, ground-response analysis, shear-wave velocity, site period

## 1 INTRODUCTION

Seismic-hazard analysis (SHA) is typically performed using ergodic ground-motion models (GMMs), wherein the site response component is derived from global data and conditioned on the time-averaged shear-wave velocity in the upper 30 meters ($V_{S30}$) and the depth to 1.0 or 2.5 kilometer per second (km/s) shear wave isosurfaces (e.g., $Z_{1.0}$ or $Z_{2.5}$). This approach is efficient and appealing in practice because limited shear-wave velocity ($V_S$) data are required and both commercial and open-source software are available to facilitate these analyses. However, in ergodic models, for a given $V_{S30}$, there is an implicit $V_S$ profile associated with the site response prediction and this profile has smooth increases of velocity with depth (Kamai et al., 2016). When a site-specific $V_S$ profile is characterized by abrupt velocity contrasts, for example at the rock-soil interface, the site response is likely to differ significantly from ergodic model predictions. This limitation of the ergodic models can be overcome by incorporating non-ergodic (NE) site response in the SHA. In principle, NE source and path terms could also be used; however, such procedures have not yet advanced to the point that practical application is reasonably achievable.

While NE SHA provides more accurate ground-motion estimates, the site characterization requirements and computational effort associated with these analyses are significantly greater than traditional, ergodic SHA. Therefore, it is incumbent upon engineers to advise owners when such effort is warranted for a specific project. To do so, engineers require an understanding of the conditions under which ergodic models perform poorly.

In this paper, we discuss two case histories from the San Francisco Bay Area in California where we performed both ergodic and NE SHA. We highlight significant differences in the ergodic and NE results and relate these to the subsurface conditions. We then discuss similarities between the two sites and general trends. Finally, we outline how an understanding of the $V_S$ profile and site period can aid in identifying when an NE SHA is most likely to yield significantly different results from the ergodic approach.

## 2 OVERVIEW OF APPROACH

NE site response analysis involves replacing the ergodic site model ($F_S$) in the GMMs with a non-ergodic model. The non-ergodic $F_S$ can be based on both a residuals analysis of local ground-motion recordings and/or simulations, which typically comprise one-dimensional ground-response analyses (GRA) (Stewart et al., 2017). The functional form of $F_S$ is shown in Equation 1.

$$F_S = F_{lin} + F_{nl} = f_1 + f_2 ln(\frac{x_{IMr}+f_3}{f_3}) \quad (1)$$

In the above equation, the site term represents the natural log of amplification relative to a reference site condition and is represented as the sum of a linear ($F_{lin}$) and nonlinear ($F_{nl}$) component. The linear component is defined by the $f_1$ parameter and the nonlinear component is defined by the $f_2$ and $f_3$ parameters. The degree of nonlinearity is dependent upon the reference site ground-motion parameter ($x_{IMr}$), which is typically taken as the peak ground acceleration (PGA). The $f_2$ term represents the slope of amplification vs ln($x_{IMr}$) and $f_3$ represents the approximate transition from linear to nonlinear behavior. The $f_3$ value is often fixed at a value of 0.1 g (Seyhan and Stewart 2014), which is the approach taken herein.

In some situations, ground-motion (GM) recordings located at or near a site of interest can be used to develop a NE $f_1$ value, but typically the GM data do not extend to sufficiently high intensities to develop NE $f_2$ and $f_3$ values. GRAs can be performed to obtain all three terms, provided that the associated epistemic uncertainties are considered. For the case studies discussed herein, we used local GM records to estimate $f_1$ and GRA to estimate $f_1$ and $f_2$ (Stewart et al., 2017).

In addition to replacing the ergodic $F_S$ with a NE $F_S$, the approach described herein involves modifying the GMM standard deviation ($\sigma$). Specifically, we considered a single-station within-event standard deviation ($\phi_{SS}$) in the analysis. The $\phi_{SS}$ excludes the site-to-site standard deviation; therefore; the NE $\sigma$ is lower than the ergodic $\sigma$. However, it is important to point out that a NE analysis requires consideration of epistemic uncertainties in the site amplification and, particularly at sites where the parameters are based solely on GRA, these epistemic uncertainties may be only modestly lower than the site-to-site standard deviations implicit to ergodic models (Stewart and Afshari, 2021).

Since both considered projects are in an area of California where the seismic hazard is controlled by shallow crustal sources, we used the following four NGA West 2 GMMs: ASK (Abrahamson et al. 2014), BSSA (Boore et al., 2014), CB (Campbell and Bozorgnia, 2014), and CY (Chiou and Yongs, 2014). We used the Third Uniform Earthquake Rupture Forecast model as implemented in the OpenSHA software.

## 3 LANDINGS CAMPUS, MOUNTAIN VIEW

The first case study that we present is the Google Landings Campus located in Mountain View, California. The campus is defined by an approximately 65,000-square-meter ($m^2$) office structure. The fundamental mode period of the structure is approximately 1.0 sec. The project is located 1.4 and 1.0 kilometers (km) from the NGA West 2 recording stations with Station Sequence Numbers (SSN) of 100003 and 100033, respectively. We denote these as Stations 1 and 2, respectively.

Subsurface conditions at the Landings Campus consist of deep soil deposits, which are made up of lean to fat clays with interbedded sands and gravels. Nearby well logs indicate that Franciscan bedrock occurs at depths of approximately 0.4 km or deeper.

### 3.1 Shear-Wave Velocity and Site Period

In Figures 1a and 1b, we present $V_S$ profiles that we developed via a joint inversion of surface-wave and horizontal-to-vertical spectral ratio (HVSR) data. We show the mean $V_S$ profile from four seismic Cone Penetration Tests (CPTs) for comparison. Due to the non-unique nature of the surface wave inverse problem, even with HVSR constraints, there is significant uncertainty in the resulting $V_S$ profiles. Accordingly, we performed multiple inversions using the "layering ratio" approach (Cox and Teague, 2016) and developed a suite of 20 $V_S$ profiles that reasonably capture this uncertainty. The $V_S$ profiles exhibit a significant impedance contrast at a depth of approximately 210 m and are consistent at shallower depths. The deeper portions of the profiles exhibit significant differences, which is typical of $V_S$ profiles derived from surface-wave testing. At depths ranging from 400-800 m, a second large impedance contrast is present, presumably due to competent Franciscan bedrock. We elected to consider these full-depth profiles in GRA, which required specific procedures to account for the fact that the $V_S$ of the bottommost layer is significantly higher than the upper limit of applicability of the GMMs in many cases. We addressed this issue in the manner described in Stewart et al. (2019). While it would be convenient and consistent with typical practice to truncate the profiles at the first impedance contrast (≈210 m), these profiles would fail to capture the fundamental period of the site.

Horizontal-to-vertical spectral ratio (HVSR) data from the project site and the nearby GM recording stations are shown in Figure 1c. The HVSR curves from the project site and GM recording stations are similar, with the lowest frequency peaks of 0.32 to 0.35 Hertz (Hz), corresponding to periods of 2.9 to 3.1 sec. Numerous studies indicate that when a strong peak is present in the HVSR data, this corresponds to the fundamental period of the site. Therefore, it is important to confirm that $V_S$ profiles used in GRA exhibit a fundamental period consistent with the HVSR data.

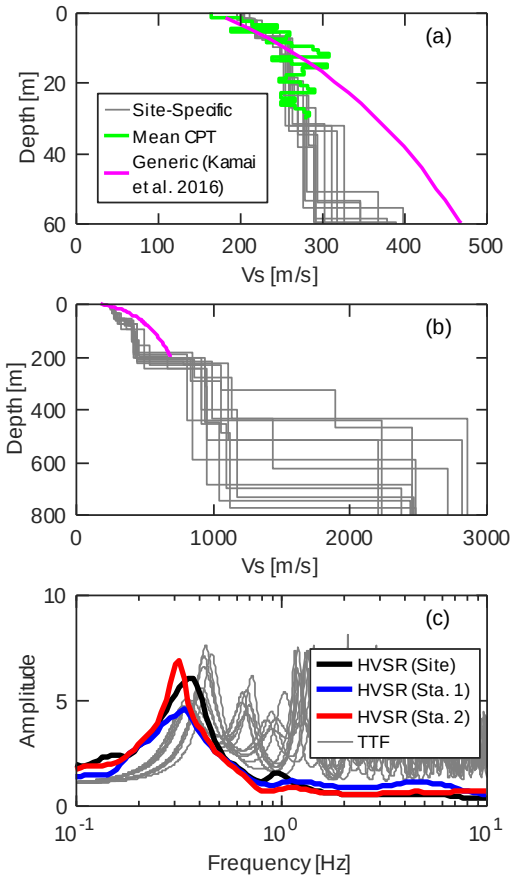


Fig. 1. $V_S$ profiles from surface-wave testing at the Landings Campus, shown to maximum depths of (a) 60 and (b) 800 meters, along with the generic $V_{S30}$ based profile from Kamai et al. (2016). In (c), the HVSR data from the project site and nearby ground-motion recording stations are compared along with the theoretical transfer functions for the $V_S$ profiles.

We present the linear, viscoelastic theoretical transfer functions (TTFs) for the $V_S$ profiles obtained from inversion in Figure 1c. The lowest frequency peak of these TTFs (i.e., the fundamental mode) varies from approximately 0.3 to 0.4 Hz, which is well aligned with the peak in the HVSR data. This is due in part to the inclusion of the HVSR data in the inversion. Note that while the lowest frequency peaks are aligned, the amplitude of the TTFs and HVSR curves do not and should not necessarily match.

The generic $V_S$ profile based on the site $V_{S30}$ of approximately 250 meters per second (m/s) is shown in Figures 1a and 1b (Kamai et al., 2016). This profile is valid to a depth of approximately 200 m. This profile is generally in poor agreement with the site-specific profiles, which exhibit a smaller velocity gradient over the upper 200 m, followed by a significant impedance contrast.

### 3.2 Residuals Analysis

In Figure 2, we present the within-event residuals computed for Stations 1 and 2 based on the BSSA GMM. These stations had 21 and 9 available low-intensity records, respectively. We did not calculate residuals at periods greater than the inverse of the lowest usable frequency denoted in the NGA West2 flatfile.

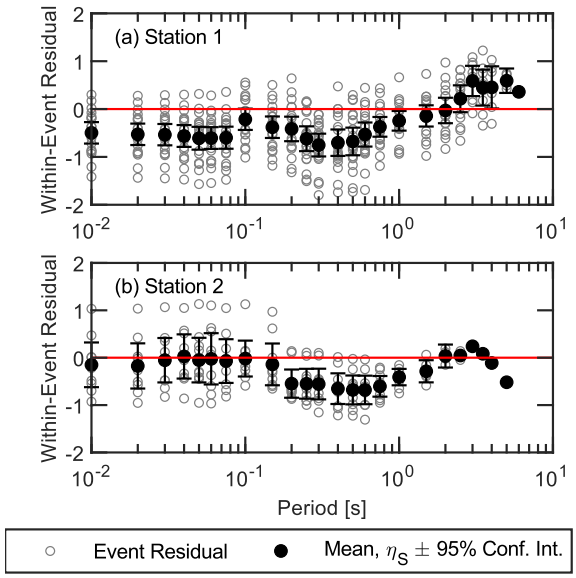


Fig. 2. Within-event residuals from (a) Station 1 and (b) Station 2 near the Landings Campus.

A residual greater than zero indicates that the GMM tends to underestimate the ground motion and vice versa. For both stations, the mean within-event residuals are negative between 0.1 and 2 seconds, indicating that the GMM tends to overestimate the ground motions for weak shaking conditions. Conversely, the within-event residuals are positive and reach a maximum at a period of approximately 3 sec, which is in very good agreement with the site period estimated from HVSR testing. We used these within-event residuals to calculate the linear $f_1$ term (Stewart et al., 2017).

### 3.3 Amplification Function Parameters

We estimated NE $f_1$ values based on both the residuals described previously and linear GRAs that we performed using the site $V_S$ profiles. We present these results, along with the ergodic $f_1$ for the site, in Figure 3. These GM- and GRA-based $f_1$ values exhibit similar trends and indicate that the ergodic model overestimates the linear amplification over a broad period range of approximately 0.15 to 2 sec and underestimates the amplification at the site period (approximately 3 sec). We calculated a weighted mean $f_1$ value for use in subsequent analyses by assigning equal weight to the values derived from Station 1, Station 2, and linear GRAs. These weights were based on site-specific considerations. Although Station 1 has more records than Station 2, we assigned equal weight to Station 2 because it is closer to the project site. The weighted mean is shown in Figure 3. At periods greater than 3 sec, we transitioned to the ergodic $f_1$ values due to limitations of GRA at periods higher than the site period and a lack of reliable GM data. In addition to the weighted mean $f_1$

value, we considered upper/lower bounds to account for epistemic uncertainty. The range of $f_1$ values that we considered in our analysis is indicated in gray in Figure 3. We developed upper/lower bounds and associated weights as described in Stewart et al. (2019).

We estimated NE $f_2$ values based on nonlinear GRAs performed using a suite of over 100 input ground motions spanning a broad range of intensity levels. The details of these analyses are beyond the scope of this paper, but we summarize the resulting $f_2$ values in Figure 4. The ergodic $f_2$ values are also shown for comparison.

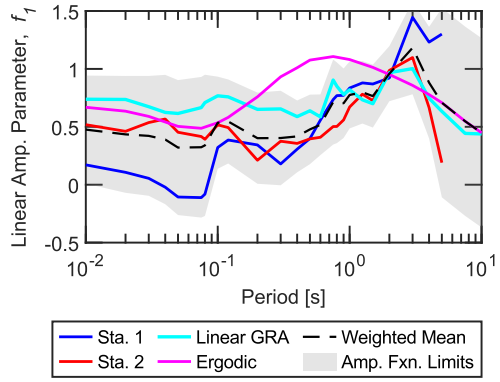


Fig. 3. Period-dependent linear amplification parameters for the Landings campus.

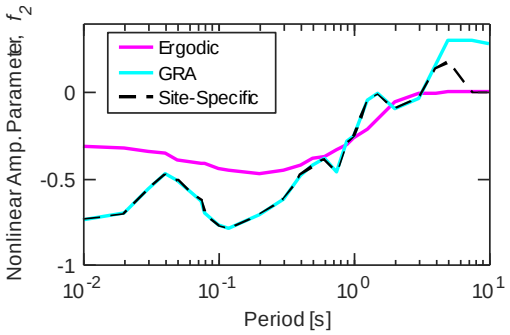


Fig. 4. Period-dependent nonlinear amplification parameters for the Landings Campus.

At periods less than 1 sec, the GRA-based $f_2$ values are significantly lower than the ergodic values. This is due in part to the presence of strong impedance contrasts in the site $V_S$ profiles that result in more strain and associated nonlinearity compared to the smooth $V_S$ gradient implicit in the ergodic model. Between 1 and 3 sec, the GRA-based $f_2$ values are similar to or slightly exceed the ergodic values. At periods greater than 3 sec, the GRA-based values become positive. These positive $f_2$ values are due to elongation of the site period (3 sec) which causes amplifications at slightly higher periods to increase with increasing ground-motion intensity. We transitioned the GRA based $f_2$ values back to the ergodic values at periods greater than the softened site period (Stewart et al., 2017). The black curve in Figure 4 incorporates this transition and was used in subsequent analyses.

### 3.4 Seismic-Hazard Analysis Results

We incorporated the previously described non-ergodic amplification function parameters along with the $\phi_{SS}$ into NE SHA. We performed both probabilistic and deterministic seismic-hazard analyses (PSHA and DSHA, respectively), as required by the California Building Code (CBC). We present the 2,475-year uniform hazard response spectra and 84$^{th}$ percentile DSHA response spectra in Figure 5. We show the mean, median, and fractiles (16$^{th}$/84$^{th}$ and 5$^{th}$/95$^{th}$ percentile), which reflect uncertainties in amplification function parameters and GMMs. As required by the CBC, we considered the mean response spectra (orange curves) for design. We show the ergodic mean (magenta curve) for comparison. In both cases the NE mean is significantly lower at periods less than approximately 2.5 sec due to linear and nonlinear amplification function parameters that are significantly lower than the ergodic values. Since the proposed structure has a fundamental period of 1 sec, the NE SHA results yielded significant reductions in the seismic demands on the structure, leading to a more efficient structural design. Conversely, the NE pseudo-spectral accelerations (PSa) are higher in the range of 3 to 5 sec because the ergodic model underestimates the GMs at the site period, and site-period elongation occurs at longer periods. For the 2,475-year UHS, the effect of the higher amplification function parameters in this period range is partially offset by the lower within-event standard deviation, as this plays a significant role at long return periods. At periods greater than 5 sec, the NE results converge to the ergodic results for reasons discussed previously.

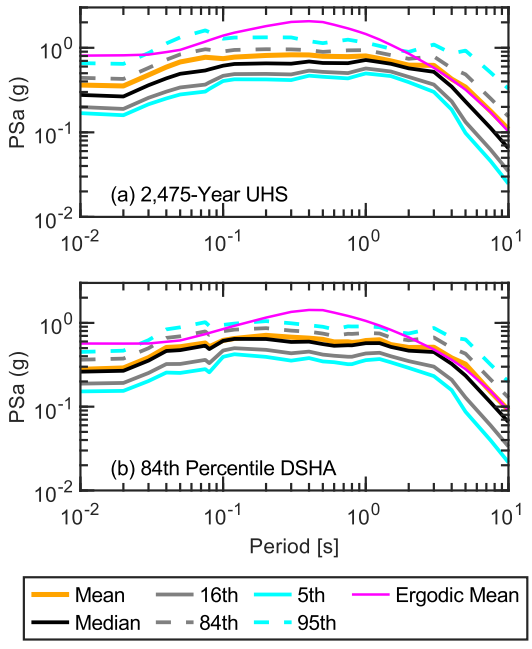


Fig. 5. Non-ergodic (a) 2,475-year uniform hazard mean response spectra and (b) 84$^{th}$ percentile deterministic response spectra for the Landings site. In each panel, the non-ergodic mean, median, and fractiles (16$^{th}$/84$^{th}$ and 5$^{th}$/95$^{th}$ percentile) representing GMM uncertainty are shown along with the ergodic mean.

## 4 ATLAS BLOCK, SAN FRANCISCO

The second case study that we present is the Atlas Block located in downtown San Francisco, California. This block consists of various structures that are undergoing seismic retrofit evaluations. One of these structures is a 34-story tower with a footprint of approximately 2,000 $m^2$. This structure is the focus herein. There are three GM recording stations located within basements or ground levels of buildings adjacent to the block, which we used in our analysis.

Subsurface conditions at the Atlas Block consist of (youngest to oldest) existing fill (Qaf), Young Bay Mud (Qybm), marine sand (Qms), Pleistocene sand (Qc), Old Bay Clay (Qobc) with dense to very dense sand interbeds (Qos), Pliestocene alluvial deposits (Qoa), and Franciscan complex bedrock (KJfs). Franciscan bedrock is at a depth of approximately 75 m beneath the 34-story tower.

### 4.1 Shear-Wave Velocity and Site Period

We performed compression- and shear-wave (PS) suspension logging in a deep borehole along with seismic cone penetration testing at the site to develop $V_S$ profiles. We present the $V_S$ data and our idealized profile in Figure 6a. There is a significant impedance contrast at the top of the Franciscan bedrock. Note that the bedrock depth in the idealized profile (75 m) is slightly shallower than the PS logging data indicate because the PS logging data were collected approximately 50 m from the 34-story building and the bedrock is deeper at that location.

We show the $V_{S30}$ based generic $V_S$ profile in Figure 6a for reference; however, it is important to point out that the $V_{S30}$ for the site is below the limits of applicability of the Kamai et al. (2016) model, because such sites are sparsely represented in the NGA West2 database. Nonetheless, the generic profile is smooth compared to the site-specific profile.

We performed HVSR testing at three onsite locations (1-HV1, 1-HV2, and 1-HV3) and two nearby ground-motion recording stations (1-HV4 and 1-HV5). As shown in Figure 6b, the HVSR results from all test locations are consistent with a lowest-frequency peak of approximately 0.8 to 1.0 Hz, corresponding to periods of 1.25 and 1.0 sec, respectively. We present the TTF for the idealized profile in Figure 6b. The lowest-frequency peak in the TTF (i.e., the fundamental mode) occurs at 0.98 Hz, which aligns with the HVSR data.

To account for uncertainty in $V_S$ in subsequent GRA, we performed randomization of the idealized $V_S$ profile with the HVSR screening criteria described in Teague et al. (2018). This approach ensures that randomized profiles are consistent with the measured site period.

### 4.2 Residuals Analysis and Amplification Function

In Figure 7, we present the within-event residuals computed using the three nearby GM recording stations based on the BSSA GMM. Records from four events were available and each event was recorded by two or more of the nearby stations. For each event, we averaged the within-event residuals from the nearby GM recording stations.

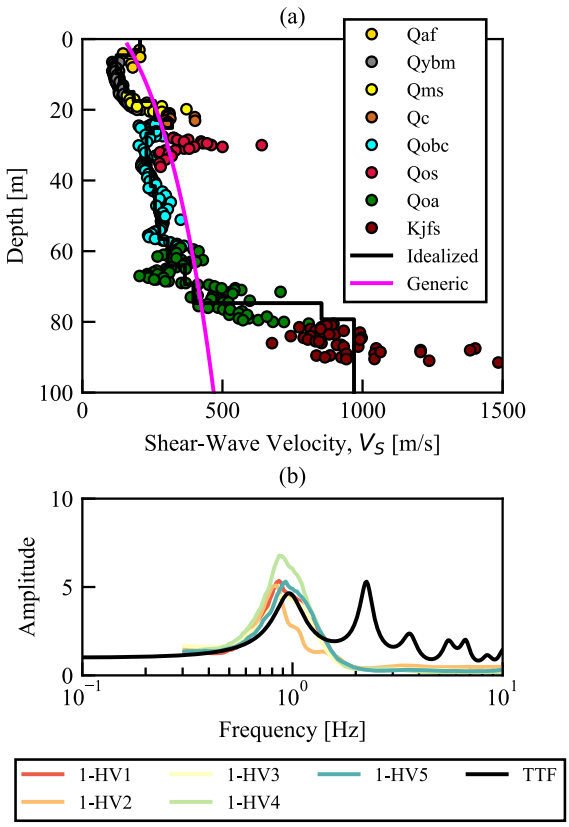


Fig. 6. (a) $V_S$ data from PS suspension logging and idealized $V_S$ profile for the Atlas Block along with the generic $V_{S30}$-based profile and (b) HVSR data recorded at and near the project site along with the TTF for the idealized $V_S$ profile for the project.

Since the available GMs were recorded in the basements or ground levels of adjacent structures, we developed transfer functions to convert the recorded foundation-level GMs to free-field GMs prior to the residuals calculation using the NIST (2012) procedures. We did not calculate residuals at periods longer than the inverse of the lowest usable frequency. As with the Landings Campus, the within-event residuals exhibit negative values (overprediction bias) at short periods and positive values (underprediction bias) in the vicinity of the site period.

We estimated the linear and nonlinear amplification function parameters ($f_1$ and $f_2$, respectively) using a similar approach to the Landings Campus. Due to space limitations, we do not present these results in this paper. However, it should be noted that the $f_1$ values exhibited similar trends to the Landings site, with positive values at/near the site period and negative values at shorter periods. The GRA-based $f_2$ values exhibited less nonlinearity than the ergodic model; however, similar to the Landings Campus, the $f_2$ values were positive at periods slightly higher than the site period due to site period elongation.

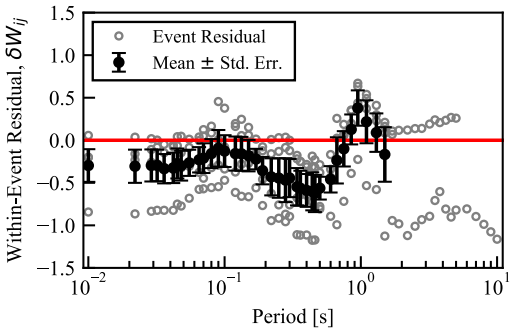


Fig. 7. Within-event residuals obtained from three ground-motion recording stations near the Atlas Block.

### 4.3 Seismic-Hazard Analysis Results

We performed NE SHA to develop 2,475-year uniform hazard response spectra and 84th percentile DSHA response spectra. We show the 2,475-year UHS in Figure 8. We show the mean, median, and fractiles along with the ergodic mean. At periods less than approximately 0.2 sec, the mean NE and ergodic response spectra (orange and magenta curves, respectively) are similar. At periods between approximately 0.2 and 0.7 sec, the NE response spectra are significantly lower. Conversely, the mean NE response spectra are significantly higher in the vicinity of the site period (1.0 sec). This is similar to the Landings Campus in that there is a broad period range below the site period where the ergodic models significantly overpredict PSa, while these models underpredict PSa at periods near the site period.

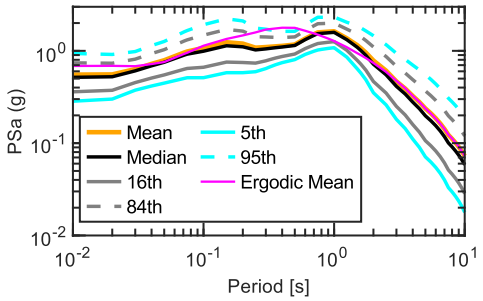


Fig. 8. Non-ergodic 2,475-year uniform hazard response spectra for the Atlas Block. In each panel, the non-ergodic mean, median, and fractiles (16th/84th and 5th/95th percentile) representing GMM uncertainty are shown along with the ergodic mean.

## 5 CONCLUSIONS

The Landings Campus and Atlas Block case studies suggest that ergodic $V_{S30}$-based site response estimates perform poorly at sites whose $V_S$ profile differs significantly from the implicit, smooth $V_S$ profile associated with the ergodic models. The non-ergodic site-response analyses from both sites exhibit similarities, suggesting that certain biases may be identified prior to performing such analyses in some cases. In particular, the $V_S$ profiles at both sites are characterized by one or more strong impedance contrasts, which result in higher amplification at site periods and lower amplification below the site period. Although deep $V_S$ profiles are often required to identify these impedance contrasts and geophysical testing to obtain these profiles can be costly, non-invasive HSVR testing can be used to readily identify whether a strong site period is present. HVSR testing is efficient, relatively inexpensive and can provide engineers with a means to identify when a non-ergodic site-response analysis and the associated geophysical testing may be of value to a project. It is important to note that both sites have unique attributes and the findings from these case histories will not necessarily apply at all sites with one or more strong impedance contrasts. Nonetheless, they provide insight that can aid in deciding whether to perform NE site-response analysis for a given project.

## ACKNOWLEDGEMENTS

The authors would like to thank the many other contributors to this work including Uri Eliahu, Pedro Espinosa, Bahareh Heidarzadeh, and Chris Nicas. We thank Google and Hines for funding the work described in the two case histories, respectively, and for recognizing the value of applying more refined SHA on their projects. We thank our colleagues who have reviewed this work for their insightful comments.

## REFERENCES

1) Abrahamson, N. A., Silva, W. J., & Kamai, R. (2014). Summary of the ASK14 ground motion relation for active crustal regions. Earthq. Spectra, 30(3).
2) Boore, D. M., Stewart, J. P., Seyhan, E., & Atkinson, G. M. (2014). NGA-West2 equ. for pred. PGA, PGV, and 5% damped PSA for shallow crust. earthqu. Earthq. Spectra, 30(3).
3) Campbell, K. W., & Bozorgnia, Y. (2014). NGA-West2 ground motion model for the average horizontal components of PGA, PGV, and 5% damped linear acceleration response spectra. Earthq. Spectra, 30(3).
4) Chiou, B. S. J., & Youngs, R. R. (2014). Update of the Chiou and Youngs NGA model for the avg. horizontal comp. of peak ground motion and response spectra. Earthq. Spectra, 30(3).
5) Cox, B. R., & Teague, D. P. (2016). Layering ratios: a systematic approach to the inv. of surface wave data in the absence of a priori information. Geophys. Journal Int., 207(1).
6) Kamai, R., Abrahamson, N. A., & Silva, W. J. (2016). $V_{S30}$ in the NGA GMPEs: Regional differences and suggested practice. Earthq. Spectra, 32(4).
7) National Inst. of Stand. and Tech (NIST). (2012). GCR 12-917-21 (2012) Soil-Structure Interaction for Bld. Structures.
8) Seyhan, E., & Stewart, J. (2014). Semi-emp. nonlin, site amp. from NGA-West2 data and simulations. Earthq. Spectra, 30(3).
9) Stewart, J. P., Afshari, K., & Goulet, C. A. (2017). Non-ergodic site res. in seismic haz. analysis. Earthq. Spec., 33(4).
10) Stewart, J. P., Wang, P., Teague, D. P., & Vecchietti, A. (2019). Applications of non-ergodic site response in ground motion modeling. Proc. of the 7th Int. Conf. on Earthq. Geotech. Eng.
11) Stewart, J. P., & Afshari, K. (2021). Epistemic uncertainty in site resp. as derived from one-dim. ground resp. analyses. Journal of Geotech. and Geoenviron. Eng., 147(1).
12) Teague, D. P., Cox, B. R., & Rathje, E. M. (2018). Meas. vs. pred. site resp. at the Garner Valley Downhole Array considering shear wave vel. uncert. from borehole and surface wave methods. Soil Dyn. and Earthq. Eng., 113.